Supplementary Information

3D-printed Acoustic Metasurface with Encapsulated Micro-air-bubbles for Frequency-Selective Manipulation

Miaomiao Ji,[ab] Yukai Liu,[ab] Zheng Zhang,[ab] Rui Xu,[a] Fanyun Pan,[a] Ya Zhang,[ab] Rouyu Su,[ab] Minghui Lu,[a] Xiujuan Zhang,[*a] and Guanghui Wang[*ab]

a. *College of Engineering and Applied Sciences, Nanjing University, Jiangsu 210093, China.*

b. *Key Laboratory of Intelligent Optical Sensing and Integration of the Ministry of Education, Nanjing University, Jiangsu 210093, China*

E-mail: xiujuanzhang@nju.edu.cn, wangguanghui@nju.edu.cn (first corresponding author).

Contents:

1 Supporting Texts

2 Supporting Figures

3 Supporting Table

4 Supporting Videos

Supporting Texts

Supplementary Note. S1: Simulation of the film vibration.

After simulating the vibration on the surface of the film, we get the vibration displacement and frequency curves approximated in the form of Gaussian function. Three cases of film vibration are constructed with three different forms of Gaussian functions.

In the case of Mode1, where the highest point of film vibration is at the center. The displacement of the highest point of film vibration is set to 1.5 μm. The bulge interval is set to 60μm. The functional equation used is:

$$D_x = 0$$

$$D_y = 1.5 * exp\left(-\frac{x^2}{2 * 30}\right)$$

In the case of mode 2, where the highest point of film vibration is off-center. The displacement of the highest point of film vibration is set to 1 μm. Set the highest point of vibration at 5μm from the center of the circle. The functional equation used is:

$$D_x = 1 * exp\left(-\frac{(x-5)^2}{2 * 30}\right)$$

$$D_y = 1 * exp\left(-\frac{(x-5)^2}{2 * 30}\right) * exp\left(\frac{\pi}{2} * i\right)$$

In the case of Mode 3, the highest point of film vibration is more off-center. The displacement of the highest point of film vibration is set to 0.5 μm. Set the highest point of vibration at 10 μm from the center of the circle. The functional equation used is:

$$D_x = 0.5 * exp\left(-\frac{(x-10)^2}{2 * 30}\right)$$

$$D_y = 0.5 * exp\left(-\frac{(x-10)^2}{2 * 30}\right) * exp\left(\frac{\pi}{2} * i\right)$$

Applying the vibrations defined by the above three functions to the film, the simulation results for Video. S1 are obtained.

Supplementary Note. S2: Discussion of the relationship between the excitation frequency f and R_{eq} for samples with different physical properties.

The relevant parameters and equations required for the calculation are given below:

Model parameters	Density ρ (Kg m^{-3})	Speed of sound c (m s^{-1})	Poisson's ratio σ	Compressibility κ (TPa^{-1})
Water	998	1495		
Polystyrene	1050	2350	0.35	249
HUVEC/3T3-L1	1200	1600	0.4	419

where κ is calculated as:

$$\kappa_{ps} = \frac{3(1-\sigma_{ps})}{1+\sigma_{ps}} \frac{1}{\rho_{ps} c_{ps}^2}$$

$$\kappa_0 = \frac{1}{\rho_0 c_0^2} = 4.48 * 10^{-10}$$

Fig.S1(a) shows the relationship between the cell's Req, excitation frequency f and the combined force $F = F_R - F_D$ was plotted using numerical analysis software. Fig.S1(b) shows the relationship between the Req and excitation frequency f of polystyrene particles and cells, respectively. At an excitation frequency of 36 kHz, the Req of the cell was about 22.4 μm.

Supplementary Note. S3: Performance of different acoustic methods in treated samples.

Comparison of the data in Table S1 shows that our study has several advantages over currently available acoustic manipulation methods. First, our chip utilizes 3D printing technology to create microholes of varying sizes, enabling selective frequency response. This contrasts with traditional bubble technology, where all bubbles are the same size and operate at the same frequency. Second, due to the dynamic tunability and stability of the bubble volume, the method in this study has a significant advantage in sample manipulation accuracy. Third, compared to existing SAW technologies capable of high-precision localized manipulation, it has a larger manipulation range, facilitates parallelization and is cheaper to produce. the present method is designed to provide higher stability of the bubble structure, which reduces the limitations of conventional microbubbles due to volume inconsistency and rupture at high power. Finally, the method of this study supports the processing diversity of cells and particles, which can be widely used in biomedical fields, especially for complex sample separation and multi-step processing processes, where traditional methods are more used for sample mixing.

Supplementary Note. S4: Temperature analysis.

In this study, three voltage conditions (10, 15, and 20 Vpp) were selected to analyze temperature changes. The excitation signal frequencies were 9 kHz and 36 kHz, respectively, and the excitation durations were both 6 minutes. As shown in Fig. S5a, the temperature changes from signal on to off were recorded for 9 sampling points in the sample chamber. Fig. S5b shows that temperature changes (ΔT) at the sampling points during excitation were less than 1°C. Figs. S5c-e illustrate the temperature variations at each sampling point under different voltage conditions at the 37 kHz excitation frequency. The results indicate that the temperature changes followed a consistent trend across different voltages, remained within the physiologically acceptable range, and did not exhibit any significant localized overheating.

Supplementary Note. S5: 3D printing model design and related parameters.

The 3D diagram of the chip design is shown in Fig. S6. The support structure, the surface patterned substrate, and sample chamber were designed to be 0.25 mm, 1.2 mm, and 120 μm thick, respectively. A total of 157 slices were obtained after slicing with 10 μm slicing software. The initial 25 slices were employed for the purpose of printing the support structure, with the print parameters set to 40 μm. The final printed support structure has a thickness of 1 mm. The next 120 slices were used to print the substrate. The first 70 slices are set to print at 40 μm and the last 50 slices are set to print at 10 μm. The final thickness of the substrate was 3.3 mm. The last 12 slices were used as prints for the sample chamber and the print parameters were set to 10 μm. The final printed sample chamber has a thickness of 120 μm. Following the removal of the supporting structure, the metasurface substrate was observed to have a thickness of 3.42 mm.

Supporting Figures

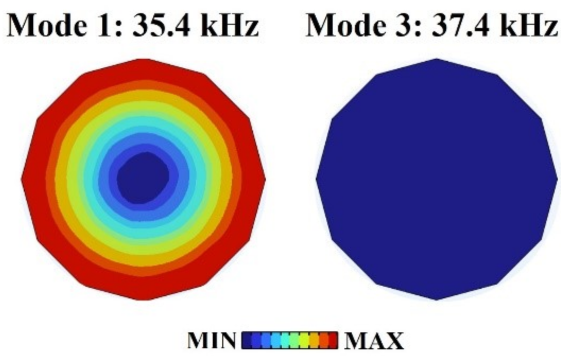

Fig. S1 The simulation results corresponding to the same values of the color bars of U.

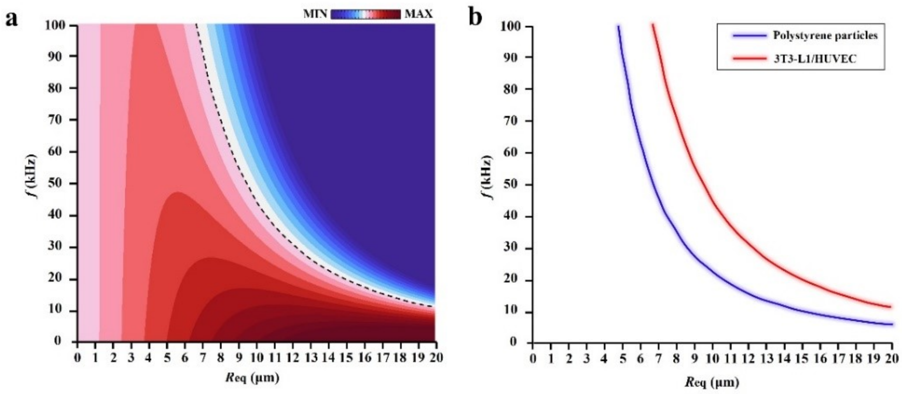

Fig. S2 (a) The relationship between the Req of 3T3-L1 cells or HUVEC cells, excitation frequency f and the combined force $F = F_R - F_D$. (b) The relationship between the Req and excitation frequency f of polystyrene particles and cells, respectively.

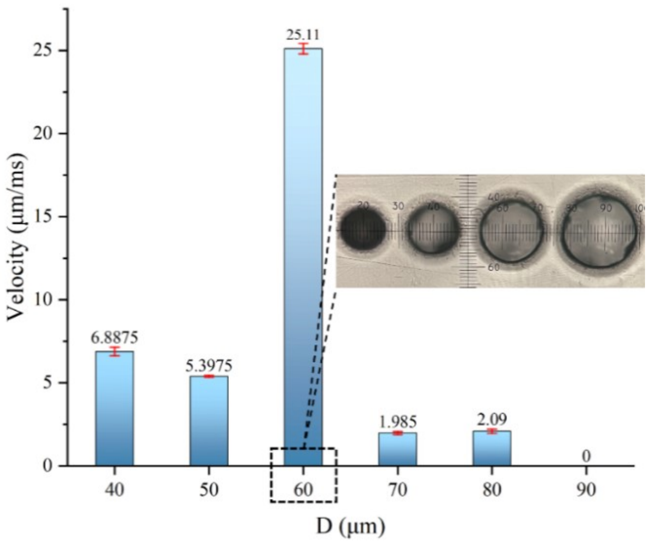

Fig. S3 Particle transport velocities at different micropore spacings D.

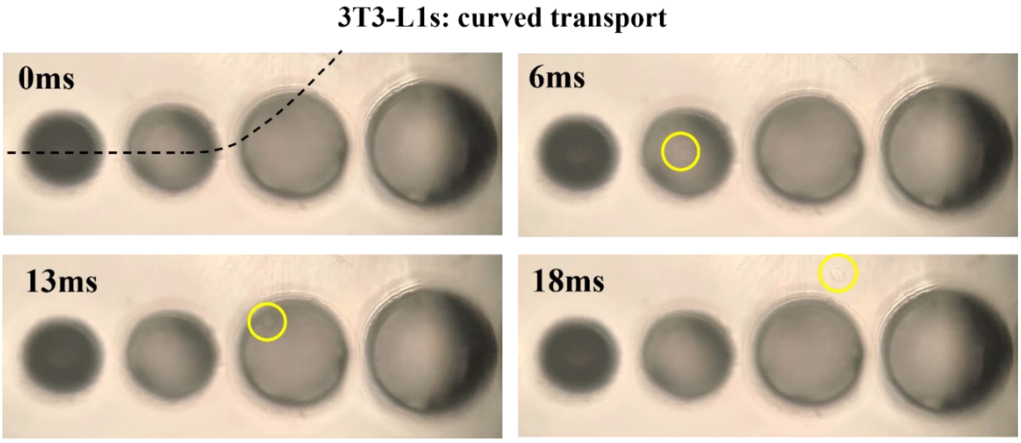

Fig. S4 The curved transport of 3T3-L1s.

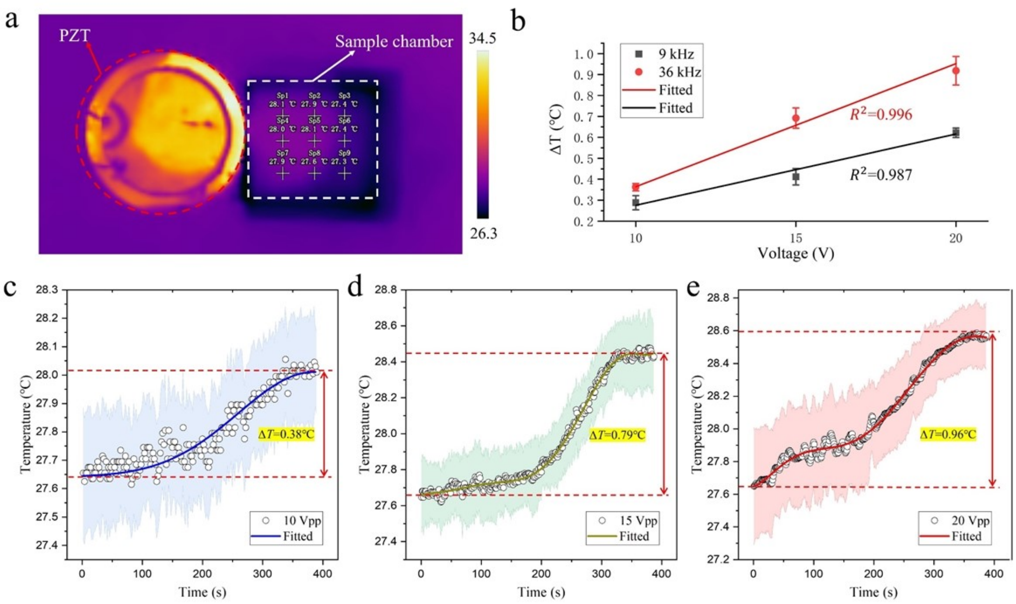

Fig. S5 Temperature test schematic and results. (a) Sampling points for temperature testing. (b) Temperature variation (ΔT) at different excitation frequencies and voltages. (c)-(e) are the temperature variation curves of the sampling points at different voltages when the excitation frequency is 36 kHz, respectively.

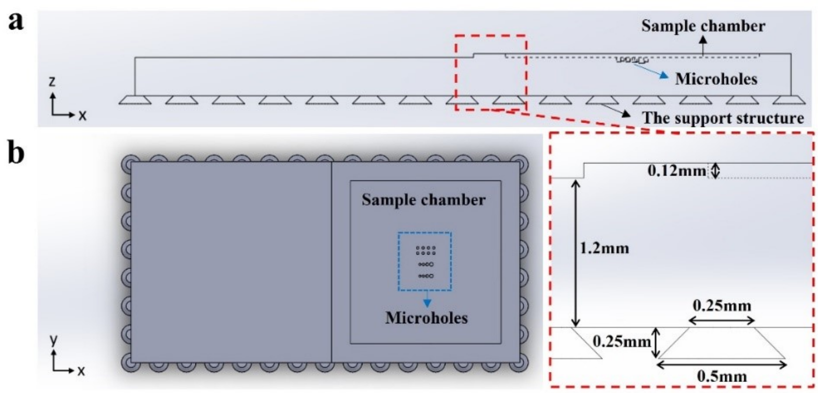

Fig. S6 (a) and (b) Schematic of 3D printing substrate design and dimensions from different viewpoints.

Supporting Table

Tab. S1: Manipulation performance of different acoustic methods.

Performance indicators	**Our Research**	**Traditional microbubble technology**[1, 2]	**Sharp edge microstructure**[3, 4]	**SAW**[5, 6]
Sample Type	cells, particles	cells, particles	particles	cells, particles
Selective Manipulation Capability	Yes	No	No	No
Precision Manipulation Capability	high	medium	medium	high
Dynamic tunability	high (Adjustable vibration direction and mode)	low	low	high
Manipulation Range	Large	Large	large	Small
Costs	low (3D printed microstructures)	high (microfabrication process)	high (microfabrication process)	high (chip Manufacturing Costs)
Stability	high	low		
Applicable Scenarios	sample concentration, sample probing, multi-step cell separation	sample mixing, single-step cell separation	sample mixing	high-precision local control

1 T. Peng, X. Lin, S. Yuan, M. Zhou, B. Jiang and Y. Jia, International *Journal of Heat and Mass Transfer*, 2023, **217**, DOI: 10.1016/j.ijheatmasstransfer.2023.124635.
2 Y. Wei, X. Lu, J. Bao, S. Zhang and D. Wu, *Advanced Materials Technologies*, 2024, **9**, DOI: 10.1002/admt.202301455.
3 W. S. Harley, K. Kolesnik, D. E. Heath and D. J. Collins, *Lab on a Chip*, 2024, **24**, 1626-1635, DOI: 10.1039/d3lc00742a.
4 X. Zhao, H. Chen, Y. Xiao, J. Zhang, S. Watanabe and N. Hao, *Materials Today Nano*, 2023, **22**, DOI: 10.1016/j.mtnano.2023.100338.
5 Y. Wang, H. Pan, D. Mei, C. Xu and W. Weng, *Lab on a Chip*, 2022, **22**, 1149-1161, DOI: 10.1039/d2lc00046f.
6 B. Aghajanloo, F. Ejeian, F. Frascella, S. L. Marasso, M. Cocuzza, A. F. Tehrani, M. H. Nasr Esfahani and D. W. Inglis, *Lab on a Chip*, 2023, **23**, 2106-2112, DOI: 10.1039/d3lc00039g.